Effect of Flap on the Wind Turbine-Concentrator Combination

E. Koç*, T. Yavuz**‡

*Department of Mechanical Engineering, Baskent University, 06790, Etimesgut, Ankara, Turkey

**Department of Mechanical Engineering, Baskent University, 06790, Etimesgut, Ankara, Turkey

(ekoc@baskent.edu.tr, tyavuz@baskent.edu.tr)

‡T. Yavuz, Department of Mechanical Engineering, Baskent University, 06790,

Etimesgut, Ankara, Turkey, Tel: +90 312 246 6666,

Fax: +90 312 246 6666, tyavuz@baskent.edu.tr

Received: 04.12.2018 Accepted:25.01.2019

Abstract- Wind energy is a renewable energy resource that can be used to ensure energy sustainability without causing environmental pollution. In this content, many studies are going on to acquire more energy from the wind. One of the methods to increase the energy production rate of the wind turbine is increasing the mass flow rate which moves through the turbine working section. This can be achieved by equipping the turbine with a concentrator. The purpose of this study is to optimize the combinations of the concentrator with flap-wind turbine leading to maximum flow speed at the turbine zone in the concentrator. Results are compared with the single airfoil type concentrator and bare turbine. The 2D CFD analyses combining the Box–Behnken Experimental Design with the Response Surface Method (RSM) are used in the optimization analyses. The actuator porous disc model is used to represent wind turbine in the concentrator. Concentrator with flap increases the flow speed by a factor of 1.2.

Keywords Concentrator, flap, optimization, response surface method, actuator disc.

Nomenclature

β	permeability
μ	dynamic viscosity
U_N	normal velocity on porous disc
U_∞	free stream velocity
U	axial velocity along the axis for verification study
S	momentum source
$P_{dyn\infty}$	dynamic pressure based on the free stream
P_{dynro}	dynamic pressure based on the flow speed on the turbine
K	resistance coefficient
ΔX_m	thickness of the porous media
C_{pj}	Porous jump coefficient
A_{ro}	area of the rotor disc
C_T	thrust coefficient
C_P	power coefficient
ε	concentrator speed-up ratio
γ	concentrator speed-up ratio without turbine ($C_T = 0$)
a	induction factor
α	concentrator angle for single airfoil type

1. Introduction

Wind power is proportional to the wind speed cubed. This means that acceleration increases the turbine energy enormously [1]. Also, by increasing flow speed the minimum start-up speed of wind or hydrokinetic turbine could be decrease. Therefore, many studies have carried out to find a

mechanism to accelerate approaching flow to the wind turbine.

A concentrator, can be used to increase the flow speed through the rotor and consequently capturing wind energy in a more efficient way [2,3]. This can be obtained by using a diffuser with/without a flanged or an airfoil shaped structure which surrounds the rotor. A flanged type concentrator generates a large separation behind concentrator, where a very low-pressure region appears to draw more flow compared to a concentrator without flange [4]. Using airfoil shaped concentrator, the mass flow rate increases through the rotor by the lift effect of airfoil [5,6]. Also adding a flap or slot behind the airfoil shaped concentrator, large concentrator exit area can be obtained without flow separation providing more mass flow rate inside the concentrator. [7,8].

Hansen et al. [9] investigated the impact of adding a concentrator around a wind turbine on turbine performance using the Computational Fluid Dynamics (CFD) model. They have shown that the Betz limit (C_{pmax} = 16/27) could be exceeded. Jamieson [10] showed that the ideal maximum power coefficient of a wind turbine driven by a concentrator is 1.5 times the Betz limit (1.5x16 / 27 = 8/9). Matsushima et al. [11] experimentally demonstrated that a wind turbine enclosed by a small-capacity flanged concentrator produces 2.4 times more energy than the turbine without flanged concentrator. Toshimitsu et al. [12] studied the performance of a wind turbine placed in a barrel with a flanged emitter using the Particle Image Velocity (PIV) technique and concluded that the wind power ratio was found to be about 2.6 times higher. Similar studies about flanged concentrator were managed by different authors [13-16]. Chen et al. [17] compared three different concentrator models positioned around small-capacity wind turbines using CFD. Results show that larger power output is obtained when the rotor placed closer to the concentrator inlet. The 60% solidity rotor, in general, achieves better power and torque outputs among the rotor solidities. Also different acceleration studies are carried out by different authors [18,19].

As the wind turbine affects the flow in the concentrator, the design of the concentrator without turbine may not be realistic. This effect can be represented by an actuator disc approach [20-23]. According to this approach the actuator disc creates the same pressure loss as wind turbine. The use of this method improves computational efficiency over a full rotor computational fluid dynamics (CFD) significantly.

The geometry and layout of the concentrator i.e. airfoil type, the position of flap with respect to main part and the flap angle highly affect the airfoil shaped concentrator performance.

Although, the effects of the design parameters on the flow through the concentrator are investigated separately, interactions between the design parameters have not been considered in present literature studies. The interactions between the design parameters are also important to reach the optimum values.

This paper includes optimum layout of the concentrator with flap-wind turbine combination to obtain maximum flow speed at turbine zone in the concentrator. Results are compared with single airfoil type concentrator and turbine without concentrator (bare turbine). The geometrical models schedule for 2D CFD analyses is obtained with the Box-Behnken Experimental Design method. The Response Surface Method (RSM) has been employed many aerodynamic works [24,25] to reveal the interactions between the design parameters. Thus, RSM is chosen to obtain the effects of the independent design parameters over the CFD results by obtaining the quadratic polynomial regression equations of average velocity at the turbine zone. Target of the paper is to use the present system to increase energy output of the wind turbine and to produce energy in the region having poor wind statistics.

2. Methodology

2.1 Geometry of Concentrator-Wind Turbine Combination

The concentrator geometry with flap is given in Fig. 1. The non-dimensional geometric parameters are defined as x/c_1, y/c_1, c_1/D, c_2/c_1, α, and δ.

- c_1 and c_2 are the chord lengths of airfoils.
- x/c_1 and y/c_1 are the ratio of the displacement of the flap with respect to main airfoil.
- α and δ is the angle of main foil and flap in relation to the free stream.
- c_1/D is the ratio of the main foil chord length to turbine diameter.
- c_2/c_1 is the ratio of the chord lengths of airfoils.

In the analyses, the diameter of the turbine rotor, D is considered to be independent variable and all variables are obtained as a function of the turbine diameter D. The analyses show that the flow speed increases linearly with the length of the concentrator [4,25]. Therefore, the c_1/D ratio is taken to be 1 and it is kept constant for a more cost-effective compact structure. As the airfoil, the SG 6043, has exclusively been used to design the small wind turbine blades and also has a high lift coefficient, this airfoil is chosen for both the main concentrator and flap [26]. The porous disc represented turbine is located at the narrowest cross-section of the concentrator with flap.

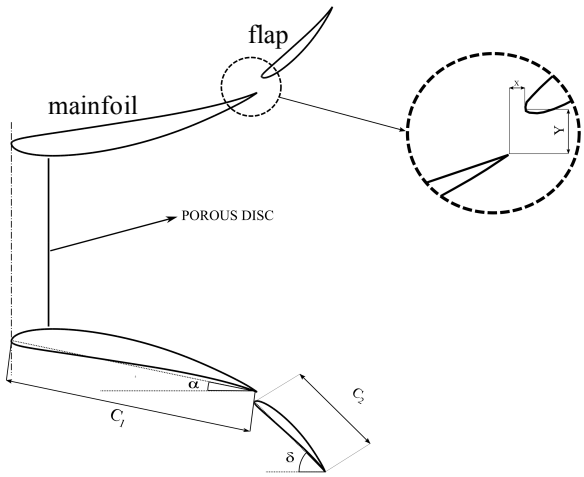

Fig. 1. Geometry and parameters of the concentrator and flap

In many researches the distance between the tip of the disc and the inside surface of the concentrator is usually chosen as is 3% of the disc radius in order to minimize tip-losses [2]. Also, porous disc thickness is selected 1% of the disc diameter [21].

2.2 Optimization Method

The response surface methodology (RSM) is used in order to reveal the effect of the parameters over the response variables and to find out the values which make the response variable among the combinations of the factor values maximum or minimum [27].

The first step in the response surface method is to determine parameters. After this step, experimental design, regression modeling, and optimization techniques are used one within another.

There are two main types of response surface designs: Central Composite Design (CCD) and Box Behnken designs. Box Behnken designs generally give fewer experiment number than CCD. Therefore, they are less expensive to run with the same number of factors.

The quadratic polynomial regression equation of velocity distribution on the porous disc derived from CFD results is in the format given by the Eq. (1) [27].

$$Y = \beta_0 + \sum_{i=1}^{k} \beta_i x_i + \sum_{i=1}^{k-1} \sum_{j=2}^{k} \beta_{ij} x_i x_j + \sum_{i=1}^{k} \beta_{ij} x_i^2 + e \qquad (1)$$

In the equation, the Y is the objective function or the predicted response which is average of the velocity distribution on the porous disc, β_0 is the offset term, βi is the linear effect, βij is the squared effect and βii is the interaction effect [27].

In this study, as c_1/D is taken to be 1, only five parameters are considered. Each parameter has three levels as low (-1), middle (0) and high (1) shown in Table 1. Referring works on the concentrator design [4,13] and on airfoil-flap design [28,29], the ranges of the parameters are chosen.

Box-Behnken experimental design method (BBD) with 5 parameters and 3 levels gives 46 experimental samples. Experimental sample schedule for CFD analyses is given in Table 2.

Table 1. Concentrator geometry parameters level for RSM

	Level 1	**Level 2**	**Level 3**
x/c_1	-3%	1%	5%
y/c_1	2%	3%	4%
α	6^o	12^o	18^o
c_2/c_1	0.3	0.35	0.4
δ	45^o	60^o	75^o

Table 2. Box-Behnken Experimental samples

	x/c_1	**y/c_1**	**α**	**c_2/c_1**	**δ**		**x/c_1**	**y/c_1**	**α**	**c_2/c_1**	**δ**
1	1	0	0	1	0	**24**	0	0	0	0	0
2	0	1	0	1	0	**25**	1	1	0	0	0
3	1	-1	0	0	0	**26**	0	0	0	0	0
4	0	0	0	0	0	**27**	0	0	1	1	0
5	0	1	1	0	0	**28**	0	1	-1	0	0
6	-1	0	0	1	0	**29**	-1	0	1	0	0
7	0	0	0	-1	-1	**30**	-1	0	-1	0	0
8	-1	0	0	0	-1	**31**	0	0	-1	-1	0
9	0	0	1	0	-1	**32**	0	-1	0	-1	0
10	1	0	-1	0	0	**33**	0	0	1	-1	0
11	0	0	0	1	-1	**34**	1	0	1	0	0
12	0	1	0	-1	0	**35**	0	0	-1	0	-1
13	0	1	0	0	1	**36**	0	0	-1	1	0
14	0	0	0	0	0	**37**	0	1	0	0	-1
15	-1	-1	0	0	0	**38**	0	0	1	0	1
16	0	0	0	0	0	**39**	0	0	0	-1	1
17	-1	0	0	0	1	**40**	1	0	0	0	-1
18	0	-1	0	0	-1	**41**	0	-1	1	0	0
19	0	-1	0	0	1	**42**	1	0	0	-1	0
20	0	-1	0	1	0	**43**	0	0	-1	0	1
21	0	-1	-1	0	0	**44**	0	0	0	1	1
22	0	0	0	0	0	**45**	-1	0	0	-1	0
23	-1	1	0	0	0	**46**	1	0	0	0	1

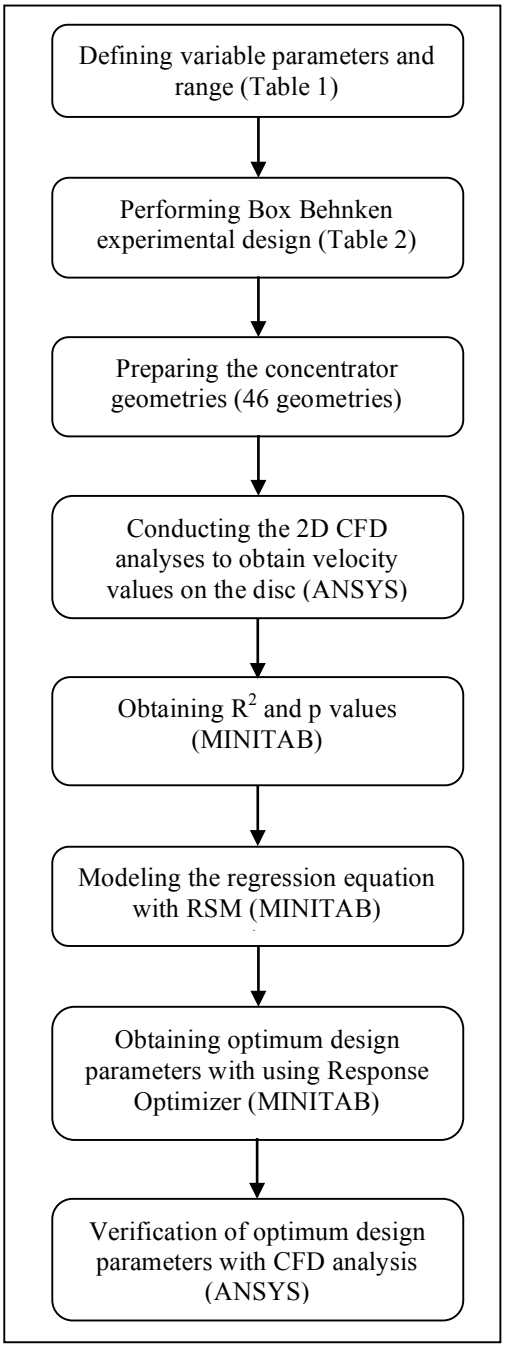

Fig. 2. Flowchart for optimization procedure

The MINITAB program is used to obtain the regression equation. The R^2 is defined as a statistical measure of how close the data fitted regression line and this value can be determined by means of MINITAB software.

The value of the R^2 is always between 0 and 1. When this value is generally closer to 1, the model is fitted to data well [30]. Also, the effect of parameters on objective function is important and p-values show this effect. If the value of the p is close to zero, the effect of the parameter shows important role on object function [30].

The optimization procedure is explained with a flow chart given in Figure 2.

2.3 CFD Analyses

CFD analyses are carried out by using ANSYS-FLUENT. The FLUENT code solves the RANS equations using finite volume method. In the analyses, RANS solution is obtained using the coupled algorithm as it offers faster convergence for steady state flows compared to the segregated solution schemes. Green-Gauss cell-based discretization method is chosen as a solver in the CFD analyses. Also, the second-order scheme is used for the momentum and turbulence equations discretization. The k-omega turbulence model has been used to solve the incompressible Navier Stokes equations. It is chosen for its ability to model boundary layer separation in adverse pressure gradients [22].

The computational domain used for the computations is shown in Fig 3. The flow is defined as axisymmetric with respect to the center axis. Different sizes of grids are used to obtain grid independency in CFD analyses. The results of the grid independence study are shown in Fig. 4.

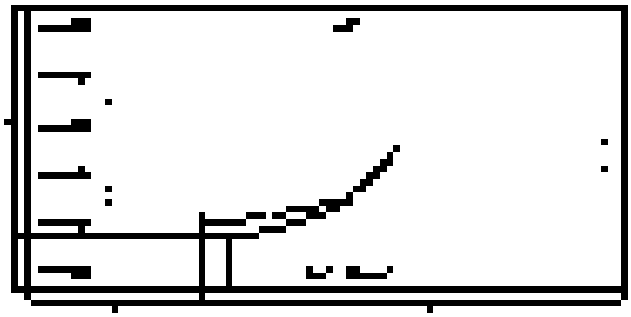

Fig 3. Structure of the computational domain

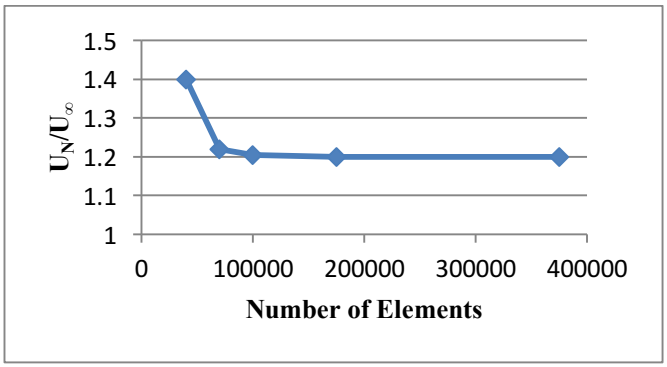

Fig. 4. Grid independency test

The quadrilateral grid structure which has better convergence and higher resolution is generated around the concentrator is shown in Fig. 5 [31].

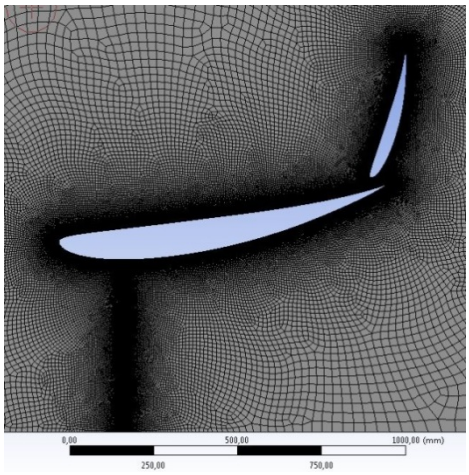

Figure 5. Mesh structure

As explained before, to find a fast and reliable approach and to solve the flow within and around the concentrator with flap, porous disc model is used with porous jump boundary conditions. The pressure drop for a porous jump, ΔP and the momentum source term, S for a homogenous porous media can be seen in Eq. (2) and Eq. (3), respectively [32]. There are three coefficients used to define the actuator disc. β is the permeability, C_{pj} is the pressure jump coefficient and ΔX_m is the thickness of the porous media.

$$\Delta P = -\left(\frac{\mu}{\beta}U_N + C_{pj}p_{dyn}\right)\Delta X_M \quad (2)$$

$$S = -\left(\frac{\mu}{\beta}U_N + C_{pj}p_{dyn}\right) \quad (3)$$

The first term of the right hand side of Eq. (2) and Eq. (3), represents the fluid flow friction through a porous media using Darcy's law. The second term represents the inertial losses to the flow as it moves through the porous media. Since the pressure loss in a turbine is proportional to the flow's dynamic head, and permeability (β) of porous jump is large enough, the viscous term is neglected [11]. Then the Eq. (2) and Eq. (3) are simplified as

$$\Delta P = -\left(C_{pj}p_{dyn}\right)\Delta X_M \quad (4)$$

$$S = -\left(C_{pj}p_{dyn}\right) \quad (5)$$

The source terms are implemented within the momentum conversion equation in the CFD code within the body force term $\bar{F}$ as

$$\frac{\delta}{\delta t}\left(\rho\vec{U}\right) + \nabla\rho\vec{U}\vec{U} = -\nabla\rho + \nabla.\left(\bar{\bar{\tau}}\right) + \rho\vec{g} + \vec{F} \quad (6)$$

which includes the other external body forces [32].

In order to make a representative turbine model implementation with porous models, the source must be related to the turbine thrust. The thrust coefficient of a turbine is given by the equation,

$$C_T = \frac{T}{p_{dyn\infty}A_{ro}} = \frac{\Delta p_{ro}}{p_{dyn\infty}} \quad (7)$$

where

$$\Delta p_{ro} = K p_{dynro} = \Delta X_M C_{pj} p_{dynro} \quad (8)$$

Assuming only inertial losses, the static pressure drop across the porous model is defined. Combining Eq. (7) with Eq. (8), the thrust coefficient can be expressed as

$$C_T = \left(\frac{{U_N}^2}{{U_\infty}^2}\right)K = \left(\frac{{U_N}^2}{{U_\infty}^2}\right)\Delta X_M C_{pj} \quad (9)$$

As can be seen in Eq. (9), the thrust coefficient is proportional to the ratio of the square of the free stream and turbine plane velocities.

The porous jump boundary condition is defined with respect to thrust coefficient as shown in Eq. (9). The one dimensional momentum analysis of the bare wind turbine and concentrator application gives the optimum value of the C_T, 0.89 leading to the maximum efficiency of turbine [9,10]. Therefore, in this optimization analysis, the optimum value of the C_T is used to be 0.89. Also, as the value of U_N is unknown, U_N^2/U_∞^2 term in the Eq. (9) is initially assumed to be 1. Then to achieve a thrust 0.89 the porous jump is specified with a thickness (ΔX_m) of 0.01m, and a pressure jump coefficient (C_{pj}) 89 m^{-1} [32].

To check whether the porous disc conditions defined properly, simple momentum theory is used [33]. In this theory, the rotational velocity component is neglected and the flow is considered to be frictionless. The control volume for the wind turbine with a simple concentrator is shown in Figure 6.

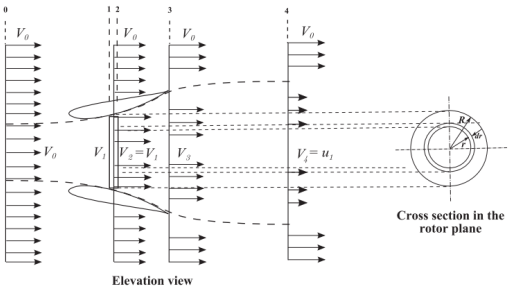

Figure 6. Simplified illustration of the velocities at the rotor plane and in the wake [16]

The velocities at the free stream, the rotor plane, the concentrator outlet and the far-wake are donated by $V_0=U_\infty$ (5 m/s) which is the general design velocity for concentrator [1] $V_1=V_2=U_N$, V_3, and V_4, respectively. There are two non-dimensional parameters; the concentrator speed-up ratios, $\gamma = U_N/U_\infty$ without turbine and $\varepsilon = U_N/U_\infty$ with turbine. The relation between ε and γ could be expressed as

$$\varepsilon = \gamma(1-a) \quad (10)$$

where a is the conventional induction factor at rotor [33,34]. Also, the thrust coefficient is given as

$$C_T = 4a(1-a) \quad (11)$$

2.4 CDF Verification

To verify the CFD analyses, a reference study [35] is used. The computational domain for reference study is given in Figure 7. Same geometry is modelled. Figure 8 shows the mesh structure for verification analysis.

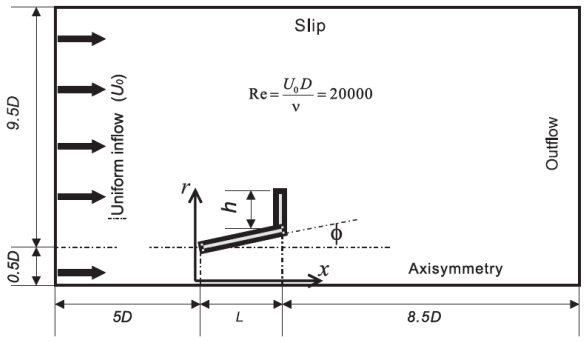

Figure 7. Computational domain of reference study [35]

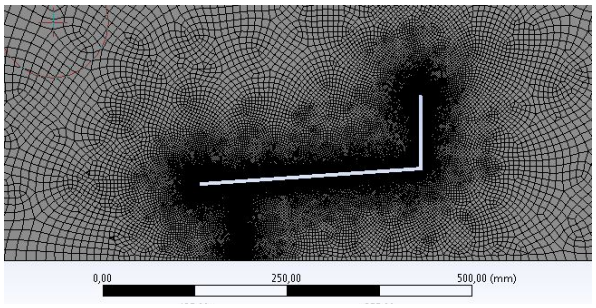

Figure 8. Mesh structure for verification analysis

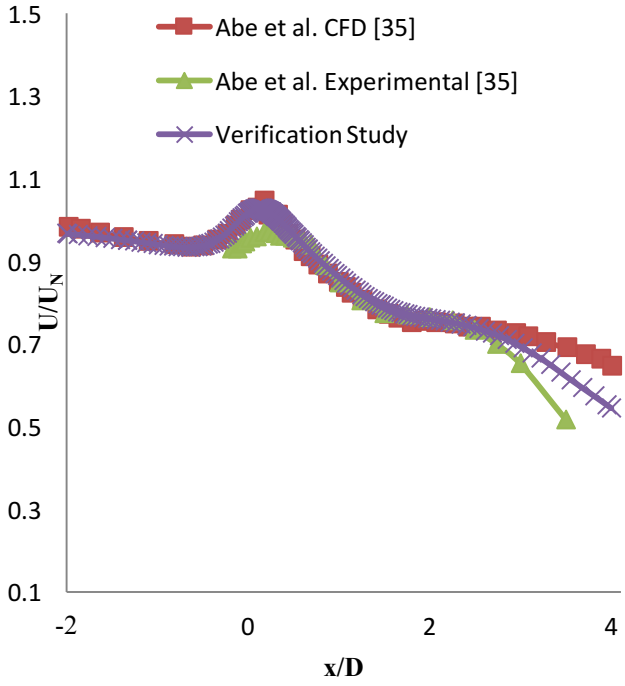

Figure 9. Velocity distribution along the center line

It is seen that disc model with porous jump being used in the present study defines properly the system and can be used for the present study.

3. Results and Discussions

After the verification, the CFD analyses are carried out for 46 samples outlined in Table 2 and the average velocities on the actuator disc are calculated. Results are given in Table 3. The regression equation given by Eq. (12), is obtained by using RSM optimization method, with respect to the CFD results.

Table 3. The results of CFD analyses.

Exp. run	Avg. Velocity(U_N) m/s	Exp. run	Avg. Velocity(U_N) m/s
1	5.91	**24**	5.85
2	5.89	**25**	5.87
3	5.89	**26**	5.85
4	5.85	**27**	5.86
5	5.80	**28**	5.73
6	5.64	**29**	5.83
7	5.88	**30**	5.24
8	5.74	**31**	5.72
9	5.80	**32**	5.78
10	5.84	**33**	5.79
11	5.92	**34**	5.84
12	5.84	**35**	5.69
13	5.89	**36**	5.76
14	5.85	**37**	5.90
15	5.62	**38**	5.83
16	5.85	**39**	5.88
17	5.63	**40**	5.90
18	5.88	**41**	5.84
19	5.93	**42**	5.85
20	5.94	**43**	5.68
21	5.77	**44**	5.92
22	5.85	**45**	5.69
23	5.72	**46**	5.91

$$Y(\text{Velocity on the porous disc}) = 5.8482 + 0.1181\ A - 0.0024\ B + 0.0738\ C + 0.0279\ D - 0.0011\ E - 0.0818\ A*A + 0.0158\ B*B - 0.0919\ C*C + 0.0144\ D*D + 0.0228\ E*E - 0.0308\ A*B - 0.1485\ A*C + 0.0269\ A*D + 0.0293\ A*E + 0.0008\ B*C - 0.0298\ B*D - 0.0161\ B*E + 0.0079\ C*D + 0.0152\ C*E + 0.0066\ D*E \quad (12)$$

The empirical Eq. (12), between the response and independent variables is determined in the coded units. A, B, C, D, E and F representing dimensionless parameters and present levels of the design parameters. The RSM method could give any value between low and high level, not the only given parameter levels value such as -1, 0, 1.

The R^2 is determined to be 0.91. As the R^2 is close to 1, regression line values are considered to be sufficient agreement with actual data. The p-values are given in Table 4.

Table 4. P-value

Parameters		P-Value
A	(x/c_1)	0
B	(y/c_1)	0.852
C	(α)	0
D	(c_2/c_1)	0.035
E	δ	0.932

As shown in table x/c_1, α, c_2/c_1 are more effective than the other parameters. The RSM with Response Optimizer tool suggests the optimum parameter levels leading to maximum velocity distribution on porous disc obtained from the regression equation (Eq. 12). These parameters are determined to be A = 1, B = -1, C = -0.2929, D = 1 and E = 1. Using linear interpolation, the real parameters can be calculated as 5% (x/c_1), 2% (y/c_1), 10.2° (α), 0.4 (c_2/c_1) and 75° (δ). Then, the optimum average velocity on porous disc is obtained to be 6.11 m/s.

Using these optimum parameters of the concentrator with wind turbine, the CFD analysis gives the maximum average wind velocity on the porous disc to be 5.95 m/s with respect to free wind velocity of 5 m/s. That means that the velocity at the turbine zone in the concentrator can be increased by 1.2 times. On the other hand, the value of the speed up ratio, γ is obtained to be 1.87 (without disc, $C_T = 0$). Also, the value of C_T (initially taken as, 0.89) is calculated and found to be as 0.92. It means that porous disc parameters are selected properly to represent the wind turbine in the concentrator.

To see the effect of the flap arrangement on the concentrator, the 2D CFD calculations are conducted on a single airfoil type concentrator without flap and wind turbine without concentrator. For single airfoil type concentrator, 6 different concentrator angles (α) 0°, 6°, 9°, 12°, 15°, 18° and 21° are chosen respectively to observe the effect of flap. The results are given in Table 5.

Table 5. Average velocity on the disc for single airfoil type concentrator

α	(U_N) m/s
0°	4.47
6°	5.05
9°	5.23
12°	5.38
15°	5.49
18°	**5.56**
21°	5.53

As seen, the maximum wind speed increase is obtained to be 5.56 m/s at the concentrator angle of α = 18°. This gives the wind speed increase by a factor of 1.1. Thus, the flap type and single airfoil type concentrators gives the velocity increase by a factor of 1.2 and 1.1 respectively.

The pressure, velocity distributions and streamline at the optimum geometric parameters for concentrator with flap-wind turbine combination and single airfoil type concentrator for 18° are shown in Fig. 10. and Fig. 11.

As shown in Figure 10, for the flap type concentrator the average pressure drop through disc is about 19.2 Pa creating average speed of 5.95 m/s on the disc, while the single airfoil type concentrator, the pressure drop is 16.8 Pa that creates flow speed of 5.56 m/s on the disc, as shown in Figure 11. The flap type concentrator has lower pressure zone behind the disc as shown in pressure contours.

Considering flow fields, it is seen that concentrator increases the flow velocity on the disc zone in both cases. Although there is no flow separation in the flap structure concentrator, there is a flow separation back side of the concentrator in the single airfoil type as shown in streamline contours. The flap accelerates the flow speed in the gap between main concentrator and flap and prevents the flow separation.

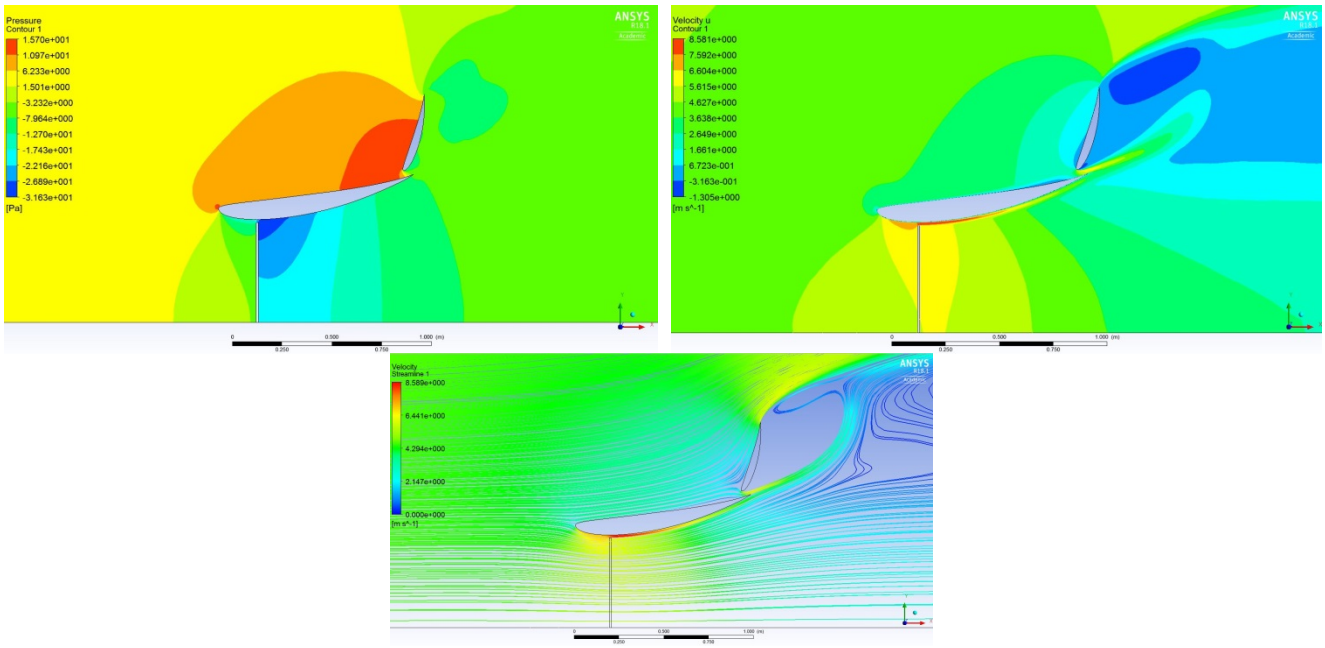

Figure 10. Pressure distribution, velocity distribution and pressure streamlines for flap type concentrator

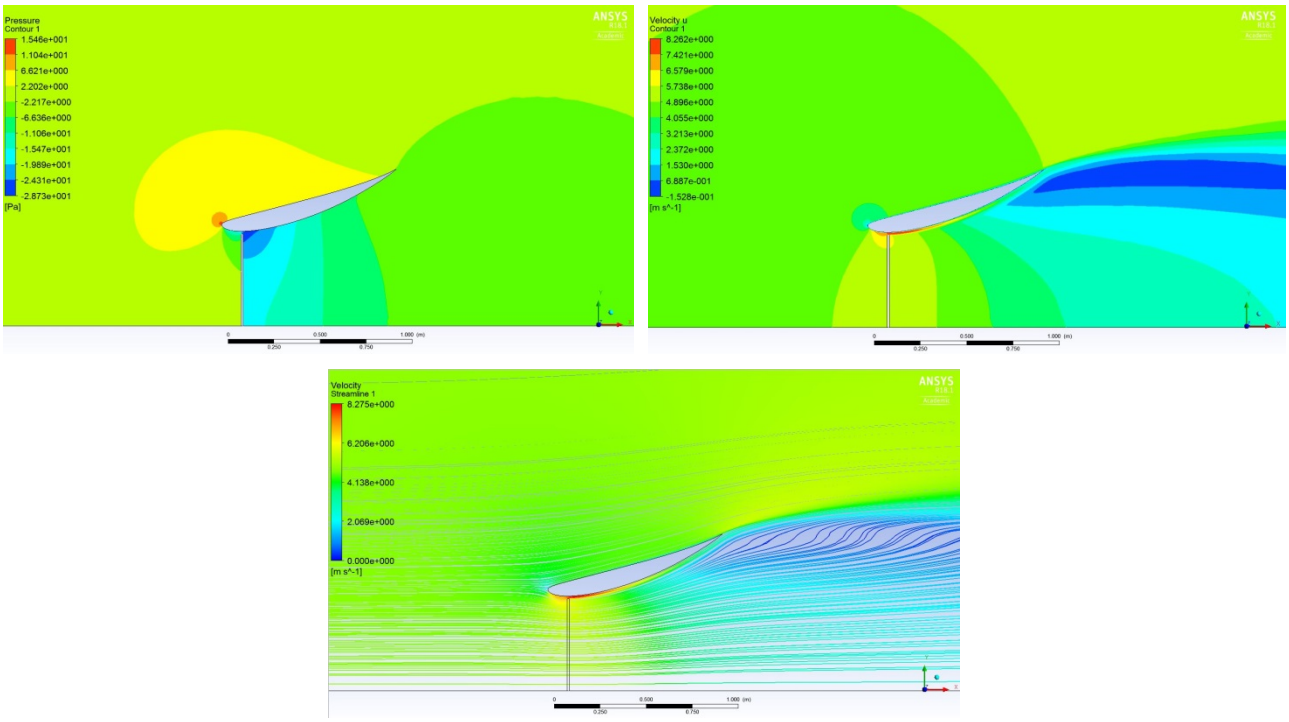

Figure 11. Pressure distribution, velocity distribution and pressure streamlines for single airfoil type concentrator

The velocity distributions along the porous disc for flap type, single airfoil type and turbine without concentrator are given in Fig.12. The location, r/R = 1 presents the edge of the porous disc (or rotor of the wind turbine). For bare turbine, the average value of the U_N/U_∞ value is obtained as 0.82. The average value of the U_N/U_∞ for concentrator with flap and single airfoil type is 1.2 and 1.1 respectively. As seen, the flap type concentrator is more effective to increase the flow speed at the turbine zone in the concentrator. In both flap and single airfoil type cases as coming closer to the diffuser wall in the radial direction, the velocity increases because of the narrowness between disc and concentrator surface and the flow at the inside surface of the concentrator is energized the boundary layer delaying the separation.

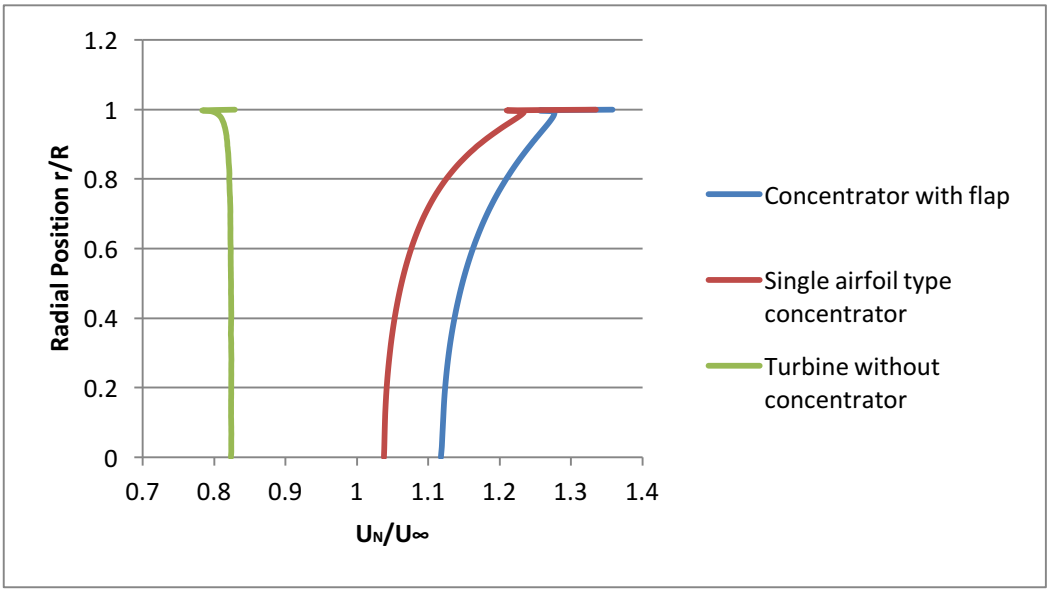

Figure 12. Velocity distributions along the porous disc for flap type, single airfoil type concentrators and turbine without concentrator

4. Conclusions

In this study, the optimum layout of the concentrator with flap-wind turbine combinations to obtain maximum flow speed increase at turbine zone is considered. Results are compared with single airfoil type concentrator and turbine without concentrator. The 2D CFD analyses combining the the Box–Behnken Experimental Design with the Response Surface Method (RSM) are used in the optimization analyses.

Conclusions drawn from the study are;

- The RSM represents a good relationship between the objective function and design parameters.
- Flap type concentrator ensures more pressure decrease behind the concentrator and consequently increases the flow speed in the concentrator leading to more energy output.
- The optimum values of the geometric parameters leading maximum flow speed at the turbine zone in the combinations of the concentrator with flap and wind turbine are 5% (x/c_1), 2% (y/c_1), 10.2^o (α), 0.4 (c_2/c_1) and 75^o (δ).
- The flap type concentrator is more effective to increase the flow speed at the turbine zone in the concentrator. It gives the velocity increase by a factor of 1.2. Also, single airfoil type concentrator gives the velocity increase by a 1.1.
- Concentrator with flap-wind turbine combination can be used to increase energy output of the wind turbine and to produce energy in the region having poor wind statistics.

Acknowledgements

Authors would like to thank to the Baskent University (BAP18/FM 16) for funding this project.

References

[1] C. Shonhiwa, G. Makaka, "Concentrator Augmented Wind Turbines: A review", Renewable and Sustainable Energy Reviews, vol. 59, pp. 1415-1418, 2016.

[2] B. L. Gilbert, K.M. Foreman, "Experiments with a diffuser-augmented model wind turbine", Journal of Energy Resources Technology", vol. 105(1), pp. 46 – 53, 1983.

[3] O. Igra, "Research and development for shrouded wind turbines", Energy Conversion and Management, vol. 21(1), pp. 13 – 48, 1981.

[4] Y. Ohya, T. Karasudani, A. Sakurai, K. ichi Abe, and M. Inoue, "Development of a shrouded wind turbine with a flanged concentrator", J. Wind Eng. Ind. Aerodyn., vol. 96(5), pp. 524-539, 2008.

[5] B. Frankovic´ and I. Vrsalovic´, "New High Profitable Wind Turbines", Renewable Energy, vol. 24(3–4), pp. 491–499, 2001.

[6] M. Shives and C. Crawford, "Developing an Empirical Model for Ducted Tidal Turbine Performance Using Numerical Simulation Results", Proc. Inst. Mech. Eng., Part A, vol. 226(1), pp. 112–125, 2011.

[7] D. Phillips, P. Richards and R. Flay, "CFD modelling and the development of the diffuser augmented wind turbine", Wind Struct., vol. 5, pp. 267–276, 2002.

[8] D. Phillips, "An investigation on diffuser augmented wind turbine design", PhD thesis, The University of Auckland, Auckland, New Zealand, 2003.

[9] M. O. L. Hansen, N. N. Sørensen, and R. G. J. Flay, "Effect of Placing a Concentrator around a Wind Turbine", Wind Energy, 2000.

[10] P. M. Jamieson, "Beating Betz: Energy Extraction Limits in a Constrained Flow Field", J. Sol. Energy Eng., vol. 131, no. 3, pp. 31008, 2009.

[11] T. Matsushima, S. Takagi, and S. Muroyama, "Characteristics of a highly efficient propeller type small wind turbine with a concentrator", Renew. Energy, vol. 31(9), pp. 1343-1354, 2006.

[12] K. Toshimitsu, K. Nishikawa, W. Haruki, S. Oono, M. Takao, and Y. Ohya, "PIV measurements of flows around the wind turbines with a flanged-concentrator shroud", J. Therm. Sci., vol. 17, pp. 375-380, 2008.

[13] Y. Ohya and T. Karasudani, "A shrouded wind turbine generating high output power with wind-lens technology", Energies, vol. 3, pp. 634-649, 2010.

[14] B. Kosasih and A. Tondelli, "Experimental study of shrouded micro-wind turbine", Procedia Engineering, vol. 49, pp. 92-98, 2012.

[15] W. X. Wang, T. Matsubara, J. Hu, S. Odahara, T. Nagai, T. Karasutani, Y. Ohya, "Experimental investigation into the influence of the flanged concentrator on the dynamic behavior of CFRP blade of a shrouded wind turbine", Renew. Energy, vol. 78, pp. 386-397, 2015.

[16] A. M. El-Zahaby, A. E. Kabeel, S. S. Elsayed, and M. F. Obiaa, "CFD analysis of flow fields for shrouded wind turbine's concentrator model with different flange angles", Alexandria Eng. J., vol. 56, No. 1, pp. 171–179, 2017.

[17] T. Y. Chen, C. W. Hung, and Y. T. Liao, "Experimental study on aerodynamics of micro-wind turbines with large-tip non-twisted blades", J. Mech., vol. 29, pp. 15-20, 2013.

[18] P. S. Narendrabhai, T. S. Desmukh, "Numerical simulation of flow through invelox wind trubine system", Int. Journal of Renewable Energy Research, vol. 1, pp. 291-301, 2018.

[19] M. Anbarsooz, M. Amiri, I. Rashidi, "A novel curtain design to enhance the aerodynamic performance of invelox: A steady-RANS numerical simulation", Energy, vol. 168, pp. 207-221, 2019.

[20] M. E. Harrison, W. M. J. Batten, L. E. Myers, and A. S. Bahaj, "Comparison between CFD simulations and experiments for predicting the far wake of horizontal axis tidal turbines", IET Renew. Power Gener., vol. 4, no. 6, pp. 613, 2010.

[21] W. M. J. Batten, M. E. Harrison, and A. S. Bahaj, "Accuracy of the actuator disc-RANS approach for predicting the performance and wake of tidal turbines", Philos. Trans. R. Soc. A Math. Phys. Eng. Sci., Vol. 371, No. 1985, pp. 20120293–20120293, 2013.

[22] V. V. Dighe, F. Avallone, J. Tang, G. J. W. Van Bussel, "Effect of gurney flap on the performance of diffuser augmented wind turbines", American Institude of Aeronautics and Astronautics, 2017.

[23] D. L. F. Gaden and E. L. Bibeau, "A numerical investigation into the effect of concentrators on the performance of hydro kinetic turbines using a validated momentum source turbine model", Renew. Energy, vol. 35(6), pp.1152-1158, 2010.

[24] B. Huang, T. Kenemoto, "Multi-objective numerical optimization of the front blade pitch angle distribution in a counter-rotating type horizontal-axis tidal turbine", Renewable Energy, vol. 81, pp. 837-844, 2015.

[25] R. Venters, B. T. Helenbrook, K. D. Visser, "Ducted wind turbine optimization" Journal of Solar Energy Engineering, vol. 140, pp. 011005– 011005–8, 2017.

[26] P. Giguère and M. S. Selig, "New airfoils for small horizontal axis wind turbines", J. Sol. Energy Eng., vol. 120, no. 2, pp. 108, 1998.

[27] B. Şimşek, Y. T. İç, and E. H. Şimşek, "A RSM-Based multi-response optimization application for determining optimal mix proportions of standard ready-mixed concrete", Arab. J. Sci. Eng., vol. 41, no. 4, pp. 1435–1450, 2016.

[28] S. Jeong, M. Murayama, and K. Yamamoto, "Efficient optimization design method using kriging model", Journal of Aircraft, vol. 42, No. 2, pp. 413-420, 2005.

[29] E. Besnard, A. Schmitz, E. Boscher, N. Garcia, and T. Cebeci. "Two-dimensional aircraft high lift system design and optimization", 36th AIAA Aerospace Sciences Meeting and Exhibit, Aerospace Sciences Meetings, 1998.

[30] Minitab R18 Support, "http://support.minitab.com/en-us/minitab/18/." 2017.

[31] D. J. Mavriplis, "Mesh generation and adaptivity for complex geometries and flows", Handbook of Computational Fluid Mechanics, Academic Press, 1996.

[32] N.W. Cresswell, "The generation potential of concentrator augmented tidal stream turbines", PhD Thesis, Durham University, 2014.

[33] J. R. P. Vaz and D. H. Wood, "Aerodynamic optimization of the blades of concentrator-augmented wind turbines", Energy Convers. Manag., vol. 123, pp. 35–45, 2016.

[34] D. A. Tavares Dias Do Rio Vaz, A. L. Amarante Mesquita, J. R. Pinheiro Vaz, C. J. Cavalcante Blanco, and J. T. Pinho, "An extension of the blade element momentum method applied to Concentrator Augmented Wind Turbines", Energy Convers. Manag., vol. 87, pp. 1116–1123, 2014.

[35] K. Abe, Y. Ohya, "An investigation of flow fields around flanged diffusers using CFD", Journal of Wind Engineering and Industrial Aerodynamics, vol. 92, pp. 315-330, 2004.